ARTICLE OPEN

Check for updates

Biosoluble ceramic fiber reinforced poly(L-lactic acid) bone scaffold: degradation and bioactivity

Cijun Shuai[1,2], Zhicheng Wang[1], Haiyang Zhang[1], Jiye Jia[1], Liping Huang[3], Dong Wang[3], Shijie Chen[3]✉ and Pei Feng[1]✉

Poly (l-lactic acid) (PLLA) exhibits great potential as a kind of scaffold material for bone defect repair because of its good biocompatibility and processability, while the too slow degradation rate hinders its further application. In this study, the biosoluble ceramic fiber (BCF) was introduced into PLLA matrix, and the PLLA/BCF composite scaffold was manufactured by selective laser sintering (SLS). It was observed that water contact angle of the composite scaffold decreased from 87.4° to 61.1° with the increasing content of BCF, while the pH value raised from 6.6 to 7.8, and the molecular weight of PLLA decreased after immersion for 4 weeks. The mechanism of degradation acceleration was that the dissolution of BCF not only released OH^- into solution environment and produced alkaline microenvironment, but also formed capillary channels on the interface between BCF and PLLA matrix, beneficial for the infiltration of water into the hydrophobic PLLA matrix, which contributed to the degradation both on the surface and in the interior of the matrix. Besides, the dissolution of BCF released Ca^{2+}, Si^{2+} and Mg^{2+} simultaneously and absorbed PO_4^{3-} from the environment, contributing to the formation of bone bonding between the scaffold and host bone. In addition, the introduced BCF improved the mechanical capacities of the scaffold via fiber breakage, fiber debond and fiber separation, and so on.

npj Materials Degradation (2022)6:87 ; https://doi.org/10.1038/s41529-022-00297-3

INTRODUCTION

The appropriate degradation rate is critical to the application of biopolymer scaffold for bone defect repair in order to avoid hindering bone tissue regeneration when degradation is too fast and failure to provide structural support when degradation is too slow[1,2]. Among various biopolymer, poly (l-lactic acid) (PLLA), with biodegradable ability, exhibits great potential as scaffold material for bone defect repair because of its good biocompatibility and processability[3–5]. It has received approval from the US Food and Drug Administration for clinical trials on human[6]. In physiological environment, the ester bonds in the PLLA chains are broken by the attack of water molecules, and long PLLA chains are broken down into short chains, which participates in the tricarboxylic acid cycle in the human body and flushed out of the body as water and carbon dioxide[7,8]. However, PLLA exhibits a slow degradation rate in the human body, more than 3 years for radical degradation, much longer than the formation rate of new bone tissue, ranging from 12 to 18 weeks[9,10].

Molecular weight of PLLA, temperature and pH of the solution environment greatly influence the hydrolytic degradation process[11–13]. For molecular weight, the degradation rate increases with the decreasing molecular weight of PLLA[14]. Tsuji et al.[15] researched on the effect of molecular weight on degradation and found PLLA with low molecular weight showed a higher molecular mobility and an increasing density of hydrophilic functional groups, enhancing the ability of water diffusion and accelerating the hydrolysis rate. Although decreasing molecular weight accelerates the degradation of PLLA, it will lead to a significant decrease of mechanical properties[16,17]. For temperature, increasing temperature can accelerate the degradation process of PLLA[18]. Weir et al.[19] researched on the degradation behavior at various temperature and found that increasing temperature could improve the movement and accelerate the random breaking of PLLA molecular chains. However, the temperature of the solution environment for degradation is limited by human body temperature, around 37 °C, when PLLA is utilized as an implant material[20]. It will damage normal cells if the environmental temperature reaches much higher than 37 °C, but it has limited effect on accelerating PLLA degradation at around 37 °C[21].

The pH value of degradation environment is also an important factor for degradation, and both acidic and alkaline mediums can accelerate the degradation rate of PLLA[22,23]. Previous studies indicate that alkaline medium has more significant catalytic effect on the PLLA degradation compared to acidic medium due to the fact that alkaline medium can neutralize the acid products from the hydrolytic degradation of PLLA[24–26]. In addition, the degradation of PLLA is a long-term process and requires a continuous alkaline medium, and an effective approach is compositing PLLA with reinforcement phase, which can increase the pH value of the degradation environment continuously[27]. Biosoluble ceramic fiber (BCF), an inorganic material composed of basic oxide (SiO_2, CaO and MgO), possesses good degradability, biocompatibility and bioactivity[28]. When the hydrophilic BCF is dissolved in the physiological environment, OH^- is released continuously and leads to an alkaline microenvironment, which can neutralize the degraded acid products of PLLA and accelerate degradation process[29]. Besides, released Ca^{2+}, Si^{2+} and Mg^{2+} contributes to absorbing PO_4^{3-} in the solution environment and forming calcium phosphate layer deposited on the surface of the scaffold, which is beneficial to the formation of a good bone bonding between the scaffold and host bone[30,31]. In addition, BCF, as a kind of fiber, plays a role of enhancement phase in the biopolymer scaffold, and bear partial stress transmitted from the matrix, through fiber breakage, fiber debond and fiber separation when the scaffold is deformed and fractured[32,33].

[1]State Key Laboratory of High Performance Complex Manufacturing, College of Mechanical and Electrical Engineering, Central South University, Changsha 410083, China. [2]Institute of Additive Manufacturing, Jiangxi University of Science and Technology, Nanchang 330013, China. [3]Department of Spine Surgery, The Third Xiangya Hospital of Central South University, Changsha 410013, China. ✉email: shijiechencsu@csu.edu.cn; fengpei@csu.edu.cn

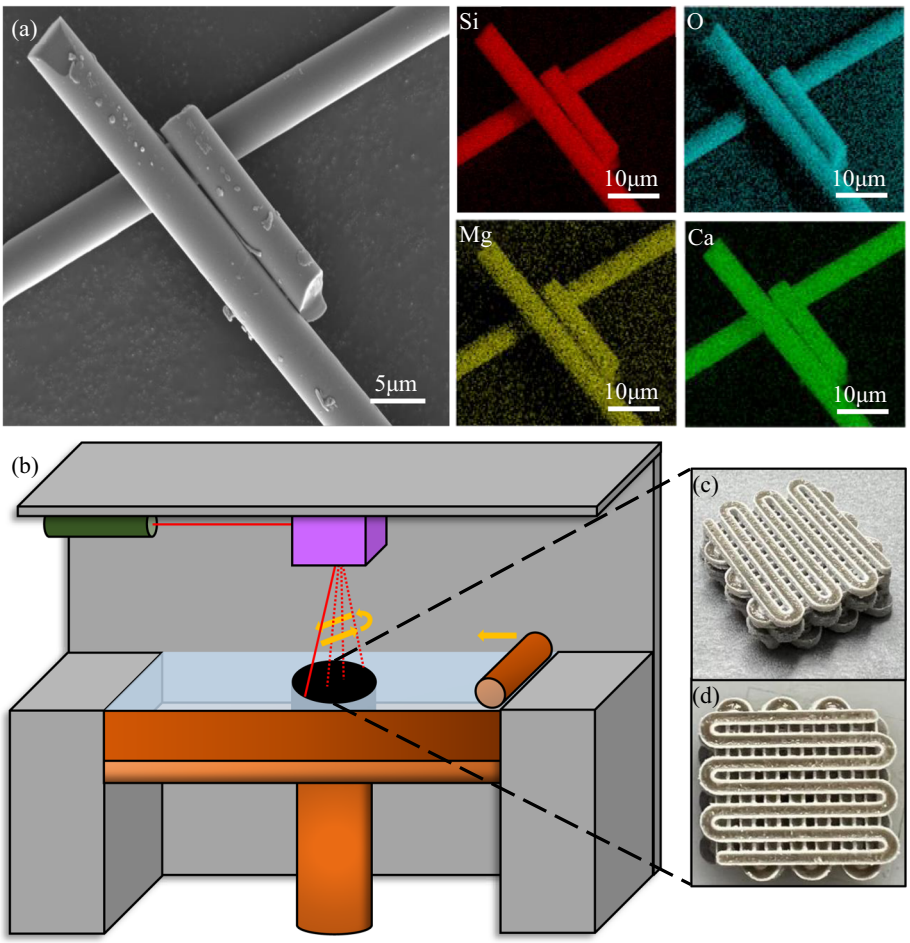

Fig. 1 Preparation and fabrication process of the scaffolds. (**a**) EDS images of BCF, (**b**) SLS process for fabricating composite scaffold, (**c**, **d**) images of the fabricated composite scaffold.

Herein, BCF was introduced to the PLLA matrix for accelerating the degradation rate of the matrix, and the composite scaffold with good bioactivity and mechanical properties was fabricated via selective laser sintering (SLS). Water contact angle experiment was executed to study the role of BCF in the hydrophilicity improvement of PLLA matrix. Immersion test was carried out to study the change of water uptake, weight loss and pH value during the process of degradation, and gel permeation chromatography (GPC) was performed to evaluate the molecular weight change of the scaffold after degradation. Tensile and compressive experiments were utilized to evaluate the mechanical properties, and scanning electron microscope (SEM) was utilized for surveying surface morphology during degradation and fracture morphology. In addition, fluorescence and cell adhesion tests were carried out to assess cytocompatibility of the composite scaffold.

RESULTS AND DISCUSSIONS

Fabrication of PLLA/BCF scaffold

BCF was brought into PLLA, and the composite scaffold was fabricated via SLS. The introduced BCF was mainly composed of SiO_2, MgO and CaO[28], and the SEM and energy dispersive spectroscopy (EDS) images were exhibited in Fig. 1a. To obtain the composite scaffold, the composite powder was put on an operation platform and spread into a layer by a roller. Then, the platform went down to 200 μm, which kept the distance between the powder layer and laser generator, as shown in Fig. 1b. The above procedures were repeated until the height of the scaffold reached desired one, and the composite scaffold in the size of 10×10×6 mm3, with horizontal and lengthwise pores, was designed and manufactured via SLS[34,35]. The fabricated PLLA/15BCF composite scaffold was presented in Fig. 1c, d, and showed a porous structure with pore size around 600 μm, holding an appropriate surface area to facilitate cell adhesion and proliferation[36,37].

Evaluation of hydrophilicity

The hydrolysis degradation is influenced by amounts of factors while the hydrophilicity is a crucial one[38]. It is a process that ester groups on PLLA chains are assailed by water molecules, and long-chain degrades to short ones and soluble substances[39,40]. Water molecules play a critical role in hydrolysis degradation process, so an excellent hydrophilicity can help scaffold absorb more water. Water climbed along the BCF surface and a funnel-shaped structure formed when BCF was in contact with water level, which indicated that BCF showed a high hydrophilicity, as shown in Fig. 2a. PLLA was usually regarded as hydrophobic material because of the few hydrophilic functional groups such as -COOH, -OH and so on, and showed the maximal water contact angle of 87.4°, as shown in Fig. 2b. When BCF was introduced into PLLA scaffold, the water contact angle value of the PLLA/BCF scaffolds decreased gradually. The PLLA/20BCF scaffold possessed the minimum water contact angle of 61.1°, which indicated that the PLLA/BCF scaffolds showed better hydrophilicity with the increase of BCF content. The improvement of hydrophilicity could be attributed that BCF consisted of a large amount of

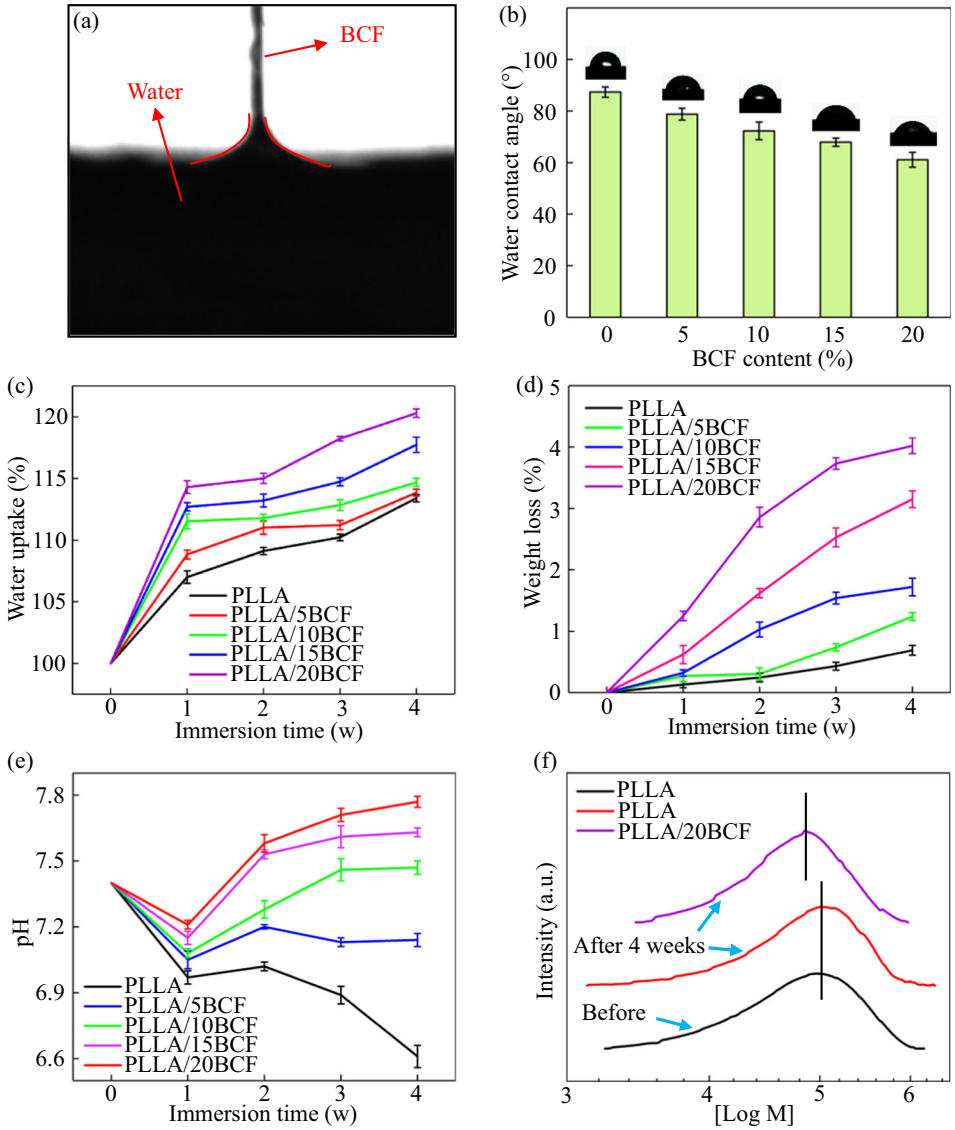

Fig. 2 Hydrophilic properties of the scaffolds. a the formation of capillary channel when BCF got to water surface, (**b**) water contact angles of the composite scaffold with different BCF content. **c** Water uptake, (**d**) weight loss and (**e**) pH variation of the composite scaffold with different BCF content during immersion in PBS, (**f**) change in M_w and molecular weight distribution of neat and composite scaffold after immersion for 4 w. The error bars represent the standard deviations from four independent specimens.

hydrophilic SiO_2 and some soluble alkaline oxides (MgO and CaO), advantageous to the dispersal of water molecules on BCF[29].

Degradation properties

Degradation properties were characterized through the variations of water uptake, weight loss, pH value, molecular weight distribution and surface morphology after immersed in PBS for 1, 2, 3 and 4 w, respectively, at 37 °C. For all scaffolds, the water absorption rate showed a progressive rise when immersion time increased and showed the maximum water uptake ratio after 4 w of immersion, but the rate of water uptake slowed down with the extension of incubation time, as shown in Fig. 2c. Weight loss rate was measured to evaluate the degree of scaffold degradation, and the results were shown in Fig. 2d. Weight loss exhibited an increasing trend as immersion time increased, and reached the maximum after incubation in PBS for 4 w. The pure PLLA scaffold possessed the minimal value of 0.7%, indicating the slow degradation rate of PLLA scaffold. The weight loss increased with increasing BCF content, and the PLLA/20BCF scaffold possessed the maximal value of 4.1%, almost six times than the PLLA one, indicating a significant expedited degradation with the introduction of BCF.

The degradation process is greatly affected by acid and alkalinity of the degradation environment, following the bulk erosion mechanism under acidic condition or the surface erosion mechanism under alkaline condition[41,42]. The former is that PLLA degrades not only superficially but also inside[43,44]. The latter is that PLLA degrades mainly ostensibly, and the average molecular weight remains steady[45,46]. The pH values of solution were measured after immersion for 1, 2, 3 and 4 w, shown in Fig. 2e. The initial pH value was 7.4, and it was found that the pH value showed a decreasing trend as immersion time increased, reaching around 6.6 after immersion for 4 w, which was attributed to the production of acidic products after degradation. For the solution containing PLLA/BCF composite scaffolds, the pH value also showed a decreasing trend after immersed for 1 w, but the pH value gradually increased and kept stable as immersion time continued increasing. The increase of pH value was attributed that the CaO and MgO in BCF could be dissolved in PBS solution and

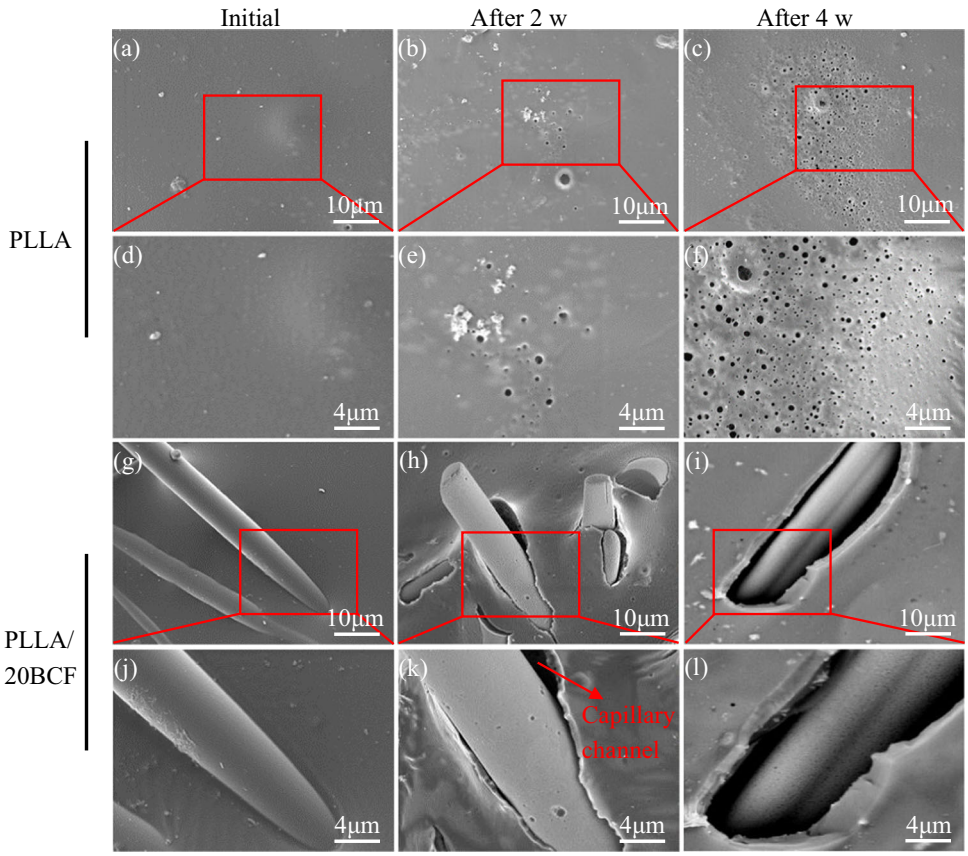

Fig. 3 Degradation morphologies of the scaffolds. Surface morphologies of (**a, d**) neat PLLA scaffold and the change in morphologies during degradation for (**b, e**) 2 weeks and (**c, f**) 4 weeks, surface morphologies of (**g, j**) PLLA/20BCF scaffold and the change in morphologies during degradation for (**h, k**) 2 weeks and (**i, l**) 4 weeks.

released OH^-, which neutralized the acidic products after PLLA degradation and led to an alkaline microenvironment. In addition, the change in pH value was related to BCF concentration, while pH value climbed up with increasing content of BCF, reaching almost 7.8 at the content of 20 wt%.

The degradation of PLLA is a process in which long PLLA chains are hydrolyzed into short ones continually[7], so it is effective to find out the effect of BCF on PLLA degradation through studying the change of molecular weight. The molecular weights before and after degradation were measured by GPC, and the results were shown in Fig. 2f. It could be observed that there was single peak in all GPC curves and almost no difference in molecular weights of PLLA before and after degradation, indicating that pure PLLA scaffold showed a poor degradation ability. But for the PLLA/20BCF scaffold, the GPC curve significantly shifted to the left, and the molecular weights of PLLA decreased after immersion in PBS for 4 w, which indicated that the introduction of BCF accelerated the degradation process of PLLA scaffold.

It is vital to observe the morphology vary in the scaffolds for evaluating the degradation properties. Degradation morphologies on the initial PLLA and PLLA/20BCF scaffolds and those after immersed for 2 and 4 w were observed by SEM, presented in Fig. 3. Before degradation, PLLA scaffold exhibited smooth and flat surface morphology, as shown in Fig. 3a, d. Immersed in PBS for 2 w later, sort of small holes appeared on the surface of the pure scaffold, as shown in Fig. 3b, e. When the immersion time reached 4 w, increasing holes emerged on the surface, and some holes were merged to form larger holes, as shown in Fig. 3c, f. For the composite scaffold, it could be observed that there were some BCFs on the surface of the scaffold, and the surface of BCF was smooth, as shown in Fig. 3g, j. There was no interspace between PLLA and BCF, which indicated good interfacial adhesion. After immersed in PBS for 2 w, sort of holes appeared on BCF superficially, and there was interspace between BCF and PLLA matrix, indicating that BCF could be dissolved in PBS, and the dissolution led to the formation of capillary channel, as shown in Fig. 3h, k. After immersed in PBS for 4 w, the interspace between BCF and PLLA matrix increased further, and the degree of degradation on BCF surface and PLLA matrix near the interface increased further, as shown in Fig. 3i, l. It could be concluded that the dissolution of BCF led to the formation of capillary channels between BCF and PLLA matrix, and water could enter into the interior of PLLA matrix along the capillary channel, which accelerated the hydrolytic degradation of PLLA matrix on the interface with BCF.

Mechanism

To better understand the mechanism of accelerating degradation, a schematic was proposed in Fig. 4. For the PLLA/BCF composite scaffold, CaO and MgO in BCF were easily dissolved in solution environment and released OH^-, which led to an alkaline microenvironment and accelerated the degradation of the matrix. Specifically, when water molecules gradually diffused into the matrix from the surface, PLLA chains were broken to soluble oligomers, such as LA, which were neutralized by OH^- in the alkaline solution. Meanwhile, interspace gradually appeared between PLLA and BCF with the dissolution of BCF, and capillary channels formed gradually, as observed by SEM test. The capillary effect of these channels promoted the diffusion of water to the interior of PLLA matrix and formed a hydrated layer, leading to the degradation in the interior of PLLA matrix. Above all. it could be concluded that degradation process was accelerated as the

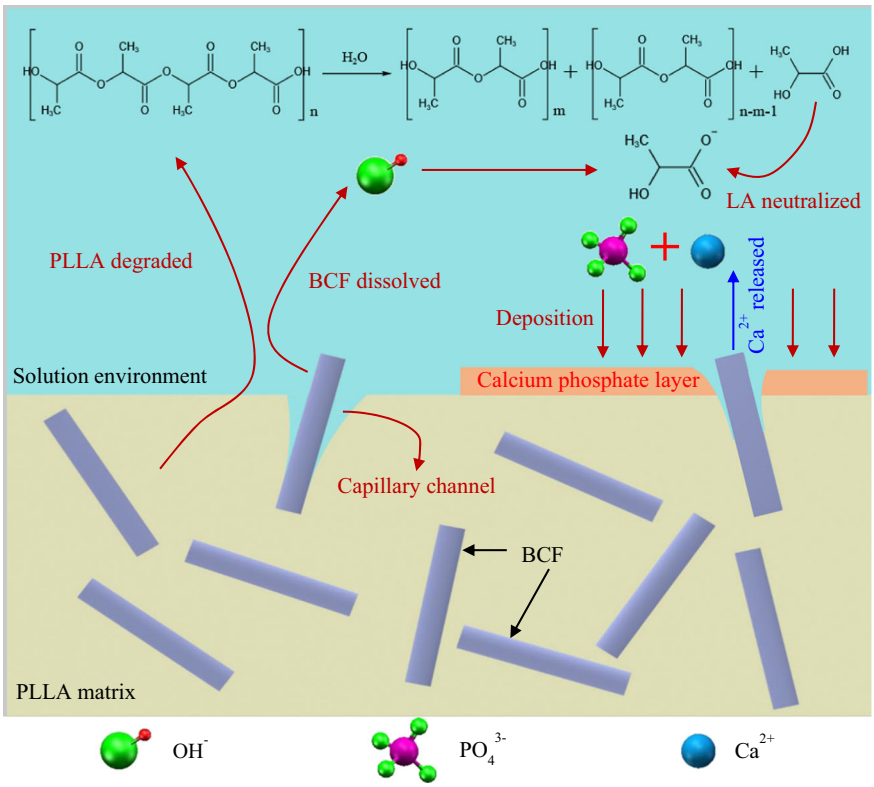

Fig. 4 Mechanism of accelerated degradation and mineralization. The mechanism of accelerating degradation for PLLA matrix and formation of calcium phosphate layer with the introduction of BCF.

degradation on the surface and in the interior of the PLLA composite scaffold proceeded simultaneously, which was consistent with the result of GPC test.

Mechanical properties

Mechanical properties are important to support the extension and breeding of osteoblasts. Dumbbell-shaped and cylindrical-shaped scaffold specimens were utilized for the tensile and compressive tests, respectively. As shown in Fig. 5a, the tensile modulus of the pure PLLA scaffold was higher than the compressive one, about 0.69 GPa and 0.47 GPa, respectively. While the content of BCF increased, both tensile and compressive moduli increased, and reached the maximum with 15 wt% BCF, about 0.97 GPa and 0.86 GPa, respectively. Specifically, the addition of BCF showed a significant effect on the improvement of compressive modulus, increasing by almost twice. In addition, the improvement effect became weak when the content of BCF reached 20 wt%. According to Fig. 5b, the tensile and compressive strength of the pure PLLA scaffold were 9.83 MPa and 20.88 MPa, respectively. After the introduction of BCF, the tensile and compressive strength of the composite scaffold were improved, and the enhancement was more obvious with the increase of BCF content. The PLLA/15BCF scaffold possessed the maximal strength of 15.01 MPa for tension and that of 35.71 MPa for compression. Compared to the pure PLLA scaffold, the tensile and compressive strength of the PLLA/15BCF scaffold increased by 52.7% and 71.1%, respectively. However, when BCF content reached 20 wt%, strengths for tension and compression decreased by 13.1% and 28.2%, respectively. Tensile and compressive tests proved that the introduction of BCF could improve the mechanical performances while the reinforcement effect might be weakened when the content of BCF was excessive.

To further study the effect of BCF introduction on mechanical properties of scaffolds, SEM was carried out for the surface morphologies of the pure PLLA, PLLA/15BCF and PLLA/20BCF scaffolds after tensile tests, as shown in Fig. 5c–j. Generally speaking, fiber can effectively enhance the mechanical properties of scaffolds as fiber can bear partial stress transmitted from polymer matrix, which increases the fracture energy of the composite scaffold[47,48]. In addition, the large aspect ratio of fiber can effectively hinder the deformation and fracture of the matrix[49]. For the PLLA scaffold, the fracture surface was smooth and flat and only a few folds appeared, as shown in Fig. 5c, g, and it was regarded as brittle fracture[50]. For the PLLA/15BCF scaffold, there appeared many exposed BCF and holes on the scaffold surface, and it could be found that the end face of BCF was very rough and irregular in shape, which was attributed to the breakage of BCF by the stress transmitted from PLLA matrix, as shown in Fig. 5d, h. There were some holes due to the fact that some BCF did not fracture as the load increased, but one end of the BCF was pulled out from the matrix, and the other end might be debonded and separated from the PLLA matrix, as shown in Fig. 5e, i. When the content of BCF reached 20 wt%, the content of BCF was so high that aggregation formed, as shown in Fig. 5f, j, resulting in stress concentration and decreasing effect on the improvement of mechanical properties.

Mineralization ability

The mineralization ability of the PLLA/15BCF scaffold was evaluated by in vitro immersion experiment. After immersion in SBF at 37 °C for 2 and 4 w, the surface morphologies of the PLLA and PLLA/15BCF scaffolds were surveyed via SEM, and distribution of elements on the surface was assessed by EDS, as shown in Fig. 6. It could be found that the surface of the PLLA scaffold was smooth initially and some holes appeared on the surface when immersion time reached 2 w and the number of holes increased with immersion of 4 w. However, there was no calcium phosphate deposition even after immersion in SBF for 4 w, as shown in Fig.

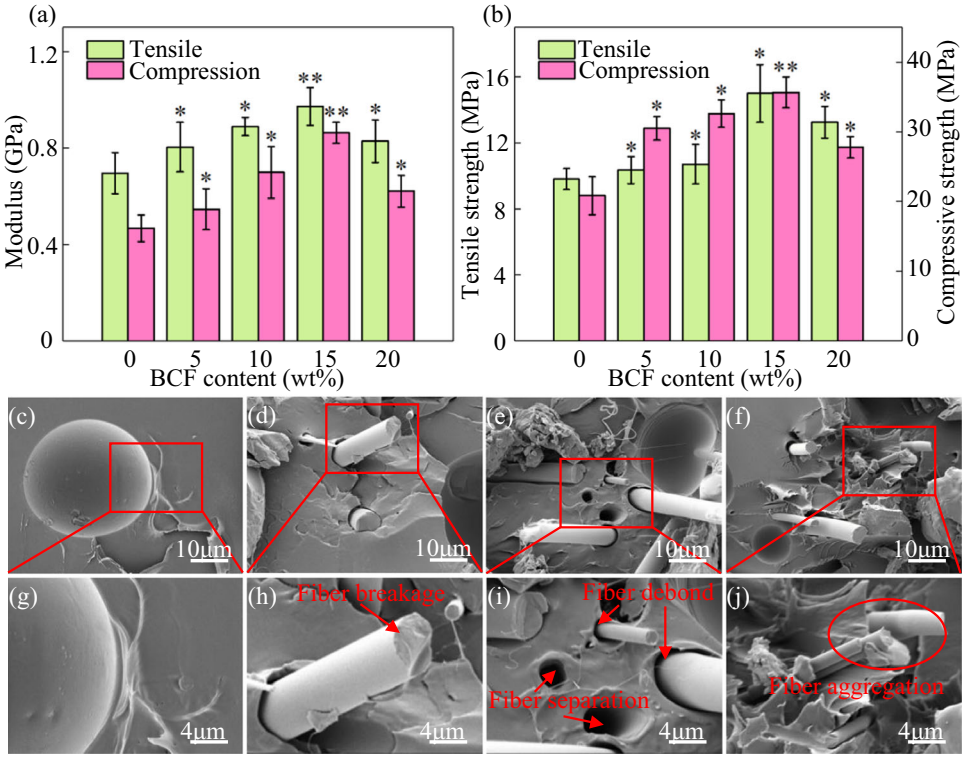

Fig. 5 Mechanical properties of the scaffolds. a Mechanical modulus and (**b**) mechanical strength of scaffolds with different BCF contents, (**c, g**) fracture morphology of the neat group, **d, h** fiber breakage, (**e, i**) fiber debond and separation occurred in the fracture of the PLLA/15BCF group and (**f, j**) fiber aggregation occurred in the fracture of the PLLA/20BCF group. * was evaluated via the t-test and indicated the statistical difference (*$p < 0.05$, **$p < 0.01$) between the composite scaffolds containing various BCF and the pure PLLA scaffold. The error bars represent the standard deviations from four independent specimens.

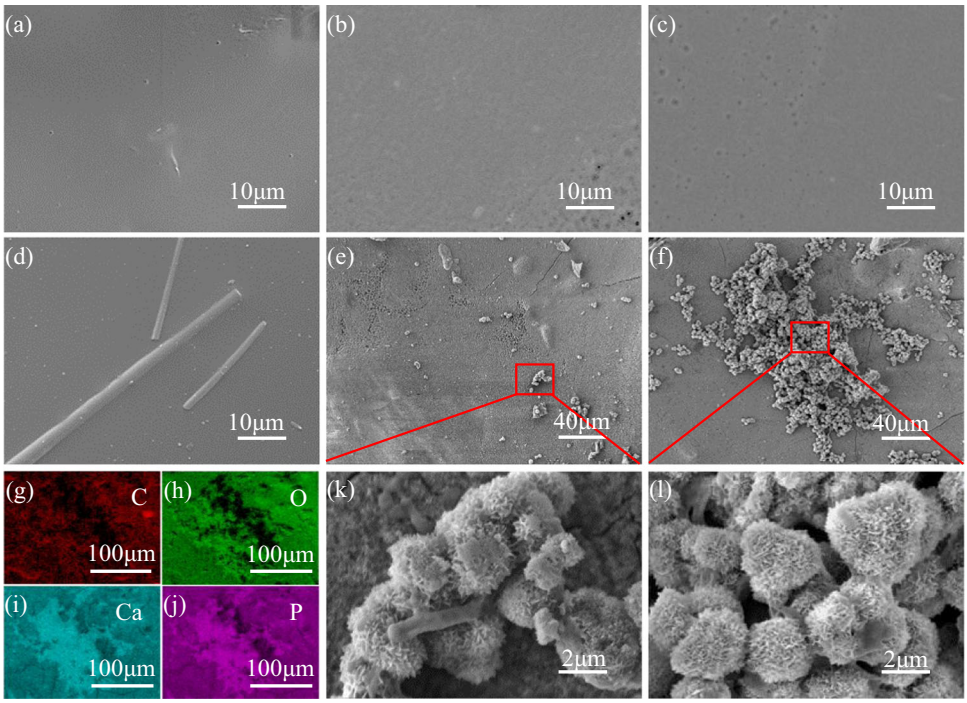

Fig. 6 Mineralization morphologies of the scaffolds. Surface morphologies for (**a**) the initial PLLA scaffold and the scaffold after (**b**) 2-week immersion and (**c**) 4-week immersion, surface morphologies for (**d**) the PLLA/15BCF scaffolds and the formation of calcium phosphate layer after (**e, k**) 2-week immersion and (**f, l**) 4-week immersion, and the EDS images of formed calcium phosphate layer for (**g**) C, (**h**) O, (**i**) Ca and (**j**) P elements.

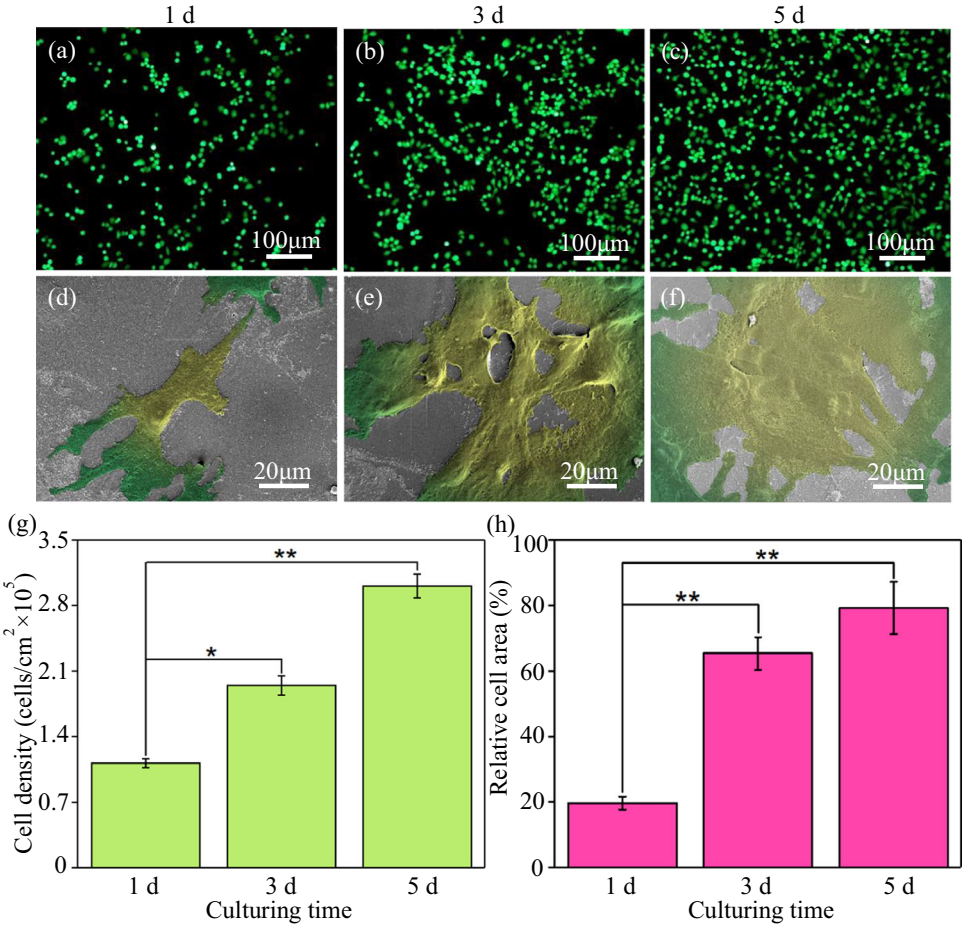

Fig. 7 Cytocompatibility of the composite scaffold. Fluorescence images of MG-63 cells cultured on PLLA/15BCF scaffold for (**a**) 1 d, (**b**) 3 d and (**c**) 5 d, cell adhesion morphologies of MG-63 cells cultured on the PLLA/15BCF scaffold for (**d**) 1 d, (**e**) 3 d and (**f**) 5 d, statistical results of (**g**) cell density and (**h**) relative cell area. * was evaluated via the t-test and indicated the statistical difference (*$p < 0.05$, **$p < 0.01$) compared with the group cultured for 1 d. The error bars represent the standard deviations from four independent specimens.

6a–c, which indicated that the PLLA scaffold didn't possess bioactivity. Compared with the morphologies of the PLLA scaffold, it could be observed that the PLLA/15BCF scaffold showed a smooth surface before immersion but the surface turned to be rough and calcium phosphate deposition appeared on the surface after immersed in SBF for 2 w, and the number of depositions climbed up with increasing immersion time, as shown in Fig. 6d–f, k, l. Further magnification showed that the deposition was made up of a large number of "cauliflower-shaped" spherical particles and formed bonding with BCF, as shown in Fig. 6k, l. The results of EDS indicated that the deposition mainly contained P and Ca elements, and there were P and Ca elements distributed on the composite scaffold superficially, indicating that the scaffold had been covered by a calcium phosphate layer, as shown in Fig. 6i, j. It could be concluded composite scaffold owned good bioactivity as BCF dissolution could release Ca^{2+}, which could combine with PO_4^{3-} in the solution environment and deposited on the scaffold superficially as calcium phosphate layer, and the mechanism was shown in Fig. 4.

Cytocompatibility

It is essential for bone scaffold to possess an excellent cytocompatibility, which can support the adhesion and growth of cells[51,52]. Fluorescence and cell adhesion tests were utilized to assess the cytocompatibility of the PLLA/15BCF composite scaffold which showed the optimal mechanical properties, shown in Fig. 7. The number of MG-63 cells grew up with the increase of culturing time, finally reaching 3×10^5 cells/cm^2 after cultured for 5 d (Fig. 7g), and there were increasing cells with filopodia when culturing time reached 3 and 5 d, as shown in Fig. 7a–c. The cell morphologies on the composite scaffold were observed via SEM, shown in Fig. 7d, e. Cells were mainly in spindle shape when cultured for 1 d and the adhesion area was only about 19.8%, as shown in Fig. 7d, h. When culturing time reached 3 d, there were many filamentous colonies on the edge of cells, and some cells began to coalesced with others, finally forming a cellular layer after cultured for 5 d, as shown in Fig. 7e, f. The results of fluorescence and cell adhesion tests indicated that the PLLA/15BCF composite scaffold showed good cytocompatibility and afford an appropriate environment for osteoblasts.

In summary, BCF was brought into matrix and the PLLA/BCF composite scaffold for bone defect repair was fabricated via SLS. The degradation properties of the composite scaffold improved with the formation of alkaline microenvironment and the improvement of hydrophilicity, while the mechanical properties improved following the fiber reinforcement mechanisms. For the improvement of degradation properties, the dissolution of BCF could not only release OH^- and construct an alkaline microenvironment, leading to the degradation of matrix surface, but also formed capillary channels, contributing to the diffusion of water along the hydrophilic surface of BCF to the interior of matrix and degradation of matrix interior. The degradation process of the PLLA scaffold was accelerated as proceeded on the surface and in the interior of the scaffold simultaneously. For the improvement of

mechanical properties, BCF could bear partial stress in the PLLA matrix and consume the fracture energy via fiber breakage, fiber separation and fiber debond. The dissolution of BCF could also release Ca^{2+}, which combined with PO_4^{3-} and formed calcium phosphate layer on the scaffold superficially. In addition, from the results of fluorescence and cell adhesion tests, it was concluded that the PLLA/BCF scaffold showed an excellent cytocompatibility, which could support the adhesion and breeding of osteoblasts. The fabricated PLLA/BCF composite scaffold, with higher biodegradation rate and improved bioactivity and mechanical properties, is a promising candidate for the application in bone defect repair.

METHODS

Materials

Powder of PLLA, with an average diameter of 150 μm, was obtained from Shenzhen Polymtek Biomaterial Co., Ltd. (Shenzhen, China). BCF was purchased from Jinan Huolong Thermal Ceramics Co., Ltd. (Jinan, China), and the aspect ratio and average diameter ranged from 10 to 20 and from 2 to 7 μm, respectively. Phosphate buffer saline (PBS), simulated body fluid (SBF) and ethanol were purchased from Sinopharm Chemical Reagent Co., Ltd. (Beijing, China).

Scaffold fabrication

PLLA and BCF were blended in ethanol and stirred magnetically for 40 min. The blended powder under weight ratio of 0:100, 5:95, 10:90, 15:85 and 20:80 (BCF/PLLA), was dried in a dry cabinet (Guangzhou, China) at 45 °C for 1 d. The scaffolds were manufactured via SLS. During the fabrication process of the scaffold, scanning rate and laser output were set to 100 mm/s and 2.3 W, and every tier was spread to about 200 μm[53–56]. To obtain a denser surface and better mechanical properties, the refill filling strategy was performed during the laser marking process of each layer, and the scanning direction altered 90° and repeated after a scanning process to get equal mechanical properties in two directions[57,58]. The composite scaffolds, prepared with BCF content of 0 wt%, 5 wt%, 10 wt%, 15 wt % and 20 wt%, were named PLLA, PLLA/5BCF, PLLA/10BCF, PLLA/15BCF and PLLA/20BCF, respectively.

Hydrophilicity

Theta Lite optical tensiometer (Stockholm, Sweden) was utilized for observing change of liquid level when BCF was in contact with it and measuring water contact angle to characterize the hydrophilic variation. All specimens were in the size of 10 mm × 10 mm × 5 mm. Angles were recorded when droplet morphology was stable.

Degradation properties

The degradation properties of scaffold were evaluated by PBS immersion tests. In detail, PLLA/BCF scaffolds ($10 \times 10 \times 5$ mm^3) were immersed in PBS at 37 °C and taken out after immersed for 1, 2, 3 and 4 w, respectively, and wiped by absorbent paper. Then scaffolds were weighed to obtain water uptake ratio, following Eq. (1)[59]:

$$R_u = (W_1 - W_0)/W_0 \times 100\% \quad (1)$$

where R_u is the water uptake ratio, W_1 is the weight after incubated in deionized water, W_0 is the original weight. After that, all scaffolds were dried at 50 °C for 1 d. Weighing them to obtain weight loss ratio, following Eq. (2)[60]:

$$R_l = (W_0 - W_2)/W_0 \times 100\% \quad (2)$$

where R_l is the mass loss ratio, W_2 is the weight after dried, and W_0 is the initial weight. The pH values of the immersion media were measured during the degradation process. The pH values were detected by a digital pH meter after immersed for 1, 2, 3 and 4 w, respectively. Besides, the molecular weight distribution and weight-average molecular weight (M_w) of PLLA and composite scaffolds were evaluated by an Agilent GPC system (Palo Alto, America). The measurement temperature was 40 °C while chloroform was utilized at flow rate of 1 mL/min. The surface morphology observation was carried out by Tescan SEM (Brno, Czech Republic). All specimens were coated with a thin layer of gold before the procedure of SEM observation and the microstructural morphologies were observed in the mode of high resolution and standard intensity, under the voltage of 10 kV.

Mechanical properties

The specimen in dumbbell shape was utilized for tensile test, and active dimensions were 14 mm in length, 2 mm in width, and 2.5 mm in height. The cylindrical specimens, in the dimensions of φ6 mm × 10 mm, were utilized for compressive tests. The tensile and compressive strength were measured by mechanical testing machine (Shandong, China), according to the GB/T 528-2009/ISO 37:2005 and GB/T 7757-2009/ISO 7743:2007 standards, respectively. Furthermore, morphologies of the tensile fracture surface were observed via SEM.

Characterization of calcium phosphate layer

PLLA and PLLA/BCF scaffolds ($10 \times 10 \times 5$ mm^3) were incubated in SBF to assess bioactivity and mineralization ability. After incubation for 2 and 4 w, scaffolds were washed for five times with deionized water and dried at 50 °C for 24 h. Surface morphology after immersion was observed via SEM, and EDS was applied to assess the distribution of O, C, Ca and P elements utilizing Tescan SEM (Brno, Czech Republic), in the mode of mapping and under the voltage of 15 kV.

Cytocompatibility

Fluorescence and cell adhesion experiments were performed for the cytocompatibility of the PLLA/15BCF scaffold specimen (10 in length, 10 mm in width, and 5 mm in thickness). All the specimens were sterilized by gradient alcohol firstly. MG-63 cells were cultured in Dulbecco's modified Eagle's medium (DMEM, HyClone, USA) at 37 °C. Then, cells were seeded, with a denseness of 2×10^5 cells/cm^2, on specimens. After cultured for 1, 3 and 5 d, respectively, the specimens were fixed in 3% glutaraldehyde for 1 h. Before the fluorescence assay, the surface of the specimen was gently rinsed with PBS, dehydrated with graded ethanol twice and put into a vacuum oven until completely dried[61–63]. The fluorescence images were obtained by using a microscope equipped with a digital camera (IX51, Olympus, Japan), in which live cells were stained into the green with calcein acetoxymethyl at 37 °C for 30 min, while the cell morphology was observed by SEM[64,65].

Statistical analysis

The final value with deviation was designated by averaging four test values. Statistical significance was evaluated via the t-test utilizing the statistical package for the social sciences (SPSS, IBM Co., USA) software. Differences were deemed statistically significant and highly one at $p < 0.05$ (*) and $p < 0.01$ (**), respectively.

DATA AVAILABILITY

The data presented in this article is available upon request to the authors.

Received: 4 August 2022; Accepted: 12 October 2022;
Published online: 07 November 2022

REFERENCES

1. Detsch, R. & Boccaccini, A. R. The role of osteoclasts in bone tissue engineering. *J. Tissue Eng. Regen. M.* **9**, 1133–1149 (2015).
2. Yang, C., Huan, Z., Wang, X., Wu, C. & Chang, J. 3D printed Fe scaffolds with HA nanocoating for bone regeneration. *ACS Biomater. Sci. Eng.* **4**, 608–616 (2018).
3. Zhang, Q. et al. Fluorescent PLLA-nanodiamond composites for bone tissue engineering. *Biomaterials* **32**, 87–94 (2011).
4. Nishida, Y. et al. Fabrication of PLLA/HA composite scaffolds modified by DNA. *Polymer* **56**, 73–81 (2015).
5. He, J. et al. Scaffold strategies for modulating immune microenvironment during bone regeneration. *Mat. Sci. Eng. C.-Mater.* **108**, 110411 (2020).
6. Nazir, F., Iqbal, M., Khan, A. N., Mazhar, M. & Hussain, Z. Fabrication of robust poly L-lactic acid/cyclic olefinic copolymer (PLLA/COC) blends: study of physical properties, structure, and cytocompatibility for bone tissue engineering. *J. Mater. Res. Technol.* **13**, 1732–1751 (2021).
7. Naseem, R., Zhao, L., Eswaran, S. K. & Willcock, H. Characterization of biodegradable poly (l-lactide) tube over accelerated degradation. *Polym. Eng. Sci.* **60**, 1430–1436 (2020).
8. Ng, W. S., Lee, C. S., Chuah, C. H. & Cheng, S. F. Preparation and modification of water-blown porous biodegradable polyurethane foams with palm oil-based polyester polyol. *Ind. Crop. Prod.* **97**, 65–78 (2017).
9. Walton, M. & Cotton, N. J. Long-term in vivo degradation of poly-L-lactide (PLLA) in bone. *J. Biomater. Appl.* **21**, 395–411 (2007).
10. Jelonek, K., Li, S., Kasperczyk, J., Wu, X. & Orchel, A. Effect of polymer degradation on prolonged release of paclitaxel from filomicelles of polylactide/poly (ethylene glycol) block copolymers. *Mat. Sci. Eng. C.-Mater.* **75**, 918–925 (2017).
11. Loo, S. C. J., Tan, H. T., Ooi, C. P. & Boey, Y. C. F. Hydrolytic degradation of electron beam irradiated high molecular weight and non-irradiated moderate molecular weight PLLA. *Acta Biomater.* **2**, 287–296 (2006).
12. Fan, Y., Nishida, H., Shirai, Y. & Endo, T. Control of racemization for feedstock recycling of PLLA. *Green. Chem.* **5**, 575–579 (2003).
13. Wang, C. H., Fan, K. R. & Hsiue, G. H. Enzymatic degradation of PLLA-PEOz-PLLA triblock copolymers. *Biomaterials* **26**, 2803–2811 (2005).
14. Loo, J. S. C., Ooi, C. P. & Boey, F. Y. C. Degradation of poly (lactide-co-glycolide) (PLGA) and poly (L-lactide)(PLLA) by electron beam radiation. *Biomaterials* **26**, 1359–1367 (2005).
15. Tsuji, H. & Miyauchi, S. Enzymatic hydrolysis of poly (lactide) s: effects of molecular weight, L-lactide content, and enantiomeric and diastereoisomeric polymer blending. *Biomacromolecules* **2**, 597–604 (2001).
16. Furukawa, T. et al. Biodegradation behavior of ultra-high-strength hydroxyapatite/poly (L-lactide) composite rods for internal fixation of bone fractures. *Biomaterials* **21**, 889–898 (2000).
17. Tsuji, H., Miyase, T., Tezuka, Y. & Saha, S. K. Physical properties, crystallization, and spherulite growth of linear and 3-arm poly (L-lactide) s. *Biomacromolecules* **6**, 244–254 (2005).
18. Zhou, Q. & Xanthos, M. Nanoclay and crystallinity effects on the hydrolytic degradation of polylactides. *Polym. Degrad. Stabil.* **93**, 1450–1459 (2008).
19. Weir, N. A., Buchanan, F. J., Orr, J. F., Farrar, D. F. & Dickson, G. R. Degradation of poly-L-lactide. Part 2: increased temperature accelerated degradation. *P. I. Mech. Eng. H.* **218**, 321–330 (2004).
20. Bobel, A. C., Lohfeld, S., Shirazi, R. N. & McHugh, P. E. Experimental mechanical testing of Poly (l-Lactide)(PLLA) to facilitate pre-degradation characteristics for application in cardiovascular stenting. *Polym. Test.* **54**, 150–158 (2016).
21. Dadbin, S. & Naimian, F. Gamma radiation induced property modification of poly (lactic acid)/hydroxyapatite bio-nanocomposites. *Polym. Int.* **63**, 1063–1069 (2014).
22. De Jong, S. J. et al. New insights into the hydrolytic degradation of poly (lactic acid): participation of the alcohol terminus. *Polymer* **42**, 2795–2802 (2001).
23. Choinska, E., Muroya, T., Swieszkowski, W. & Aoyagi, T. Influence of macromolecular structure of novel 2-and 4-armed polylactides on their physicochemical properties and in vitro degradation process. *J. Polym. Res.* **23**, 1–11 (2016).
24. Numata, K. et al. Branched poly (lactide) synthesized by enzymatic polymerization: Effects of molecular branches and stereochemistry on enzymatic degradation and alkaline hydrolysis. *Biomacromolecules* **8**, 3115–3125 (2007).
25. Shirahase, T. et al. Miscibility and hydrolytic degradation in alkaline solution of poly (l-lactide) and poly (p-vinyl phenol) blends. *Polym. Degrad. Stabil.* **92**, 1626–1631 (2007).
26. Zhao, Y. et al. The degradation properties of MgO whiskers/PLLA composite in vitro. *Int. J. Mol. Sci.* **19**, 2740 (2018).
27. Wu, Z. et al. Biomimetic and osteogenic 3D silk fibroin composite scaffolds with nano MgO and mineralized hydroxyapatite for bone regeneration. *J. Tissue Eng.* **11**, 2041731420967791 (2020).
28. Liu, H., Wang, X., Zhang, B., Wang, Z. & Yang, Y. Structure and properties of CaO-MgO-SiO_2 inorganic glass fiber with additives (Al_2O_3, Y_2O_3). *J. Wuhan. Univ. Technol.* **27**, 58–62 (2012).
29. Ahmed, I. et al. Weight loss, ion release and initial mechanical properties of a binary calcium phosphate glass fibre/PCL composite. *Acta Biomater.* **4**, 1307–1314 (2008).
30. Hamai, R., Shirosaki, Y. & Miyazaki, T. Structural effects of sulfur-containing functional groups on apatite formation on Ca^{2+}-modified copolymers in a simulated body environment. *ACS Omega* **3**, 5627–5633 (2018).
31. Okuzu, Y. et al. Strontium and magnesium ions released from bioactive titanium metal promote early bone bonding in a rabbit implant model. *Acta Biomater.* **63**, 383–392 (2017).
32. Lehtonen, T. J., Tuominen, J. U. & Hiekkanen, E. Resorbable composites with bioresorbable glass fibers for load-bearing applications. In vitro degradation and degradation mechanism. *Acta Biomater.* **9**, 4868–4877 (2013).
33. Felfel, R. M. et al. Cytocompatibility, degradation, mechanical property retention and ion release profiles for phosphate glass fibre reinforced composite rods. *Mat. Sci. Eng. C.-Mater.* **33**, 1914–1924 (2013).
34. Gu, D. et al. Effects of laser scanning strategies on selective laser melting of pure tungsten. *Int. J. Extrem. Manuf.* **2**, 025001 (2020).
35. Feng, P. et al. Vertical and uniform growth of MoS2 nanosheets on GO nanosheets for efficient mechanical reinforcement in polymer scaffold. *Virtual Phys. Prototy*. https://doi.org/10.1080/17452759.2022.2115384 (2022).
36. Luo, C. et al. Influence of porous tantalum scaffold pore size on osteogenesis and osteointegration: A comprehensive study based on 3D-printing technology. *Mat. Sci. Eng. C.-Mater.* **129**, 112382 (2021).
37. Liu, R. et al. Effects of pore size on the mechanical and biological properties of stereolithographic 3D printed HAp bioceramic scaffold. *Ceram. Int.* **47**, 28924–28931 (2021).
38. Itävaara, M., Karjomaa, S. & Selin, J. F. Biodegradation of polylactide in aerobic and anaerobic thermophilic conditions. *Chemosphere* **46**, 879–885 (2002).
39. Li, J. et al. Synthesis, crystallization and hydrolysis of aromatic–aliphatic copolyester: poly (trimethylene terephthalate)-co-poly (l-lactic acid). *Polym. Degrad. Stabil.* **96**, 991–999 (2011).
40. Chang, H. M., Huang, C. C., Tsai, H. C., Imae, T. & Hong, P. D. Characterization and morphology analysis of degradable poly (l-lactide) film in in-vitro gastric juice incubation. *Appl. Surf. Sci.* **262**, 89–94 (2012).
41. Oyama, H. T., Kimura, M., Nakamura, Y. & Ogawa, R. Environmentally safe bioadditive allows degradation of refractory poly (lactic acid) in seawater: Effect of poly (aspartic acid-co-l-lactide) on the hydrolytic degradation of PLLA at different salinity and pH conditions. *Polym. Degrad. Stabil.* **178**, 109216 (2020).
42. Qiu, Z. & Pan, H. Preparation, crystallization and hydrolytic degradation of biodegradable poly (l-lactide)/polyhedral oligomeric silsesquioxanes nanocomposite. Compos. *Sci. Technol.* **70**, 1089–1094 (2010).
43. Xu, Q., Chin, S. E., Wang, C. H. & Pack, D. W. Mechanism of drug release from double-walled PDLLA (PLGA) microspheres. *Biomaterials* **34**, 3902–3911 (2013).
44. Ravi, P., Shiakolas, P. S. & Welch, T. R. Poly-l-lactic acid: pellets to fiber to fused filament fabricated scaffolds, and scaffold weight loss study. *Addit. Manuf.* **16**, 167–176 (2017).
45. Boimvaser, S., Mariano, R. N., Turino, L. N. & Vega, J. R. In vitro bulk/surface erosion pattern of PLGA implant in physiological conditions: a study based on auxiliary microsphere systems. *Polym. Bull.* **73**, 209–227 (2016).
46. Habraken, W. J. E. M. et al. In vivo degradation of calcium phosphate cement incorporated into biodegradable microspheres. *Acta Biomater.* **6**, 2200–2211 (2010).
47. Ming, R. et al. Flax fiber-reinforced polylactide stereocomplex composites with enhanced heat resistance and mechanical properties. *Polym. Composite.* **38**, 472–478 (2017).
48. Hazwani, F. & Todo, M. Characterization of bending behavior of hydroxyapatite/biopolymer porous composite beams. *Compos. Commun.* **25**, 100747 (2021).
49. Ngaowthong, C. et al. Recycling of sisal fiber reinforced polypropylene and polylactic acid composites: Thermo-mechanical properties, morphology, and water absorption behavior. *Waste Manag.* **97**, 71–81 (2019).
50. Zhang, Q. et al. Mechanical properties and biomineralization of multifunctional nanodiamond-PLLA composites for bone tissue engineering. *Biomaterials* **33**, 5067–5075 (2012).
51. Yang, Y. et al. In Situ Growth of a Metal–Organic Framework on Graphene Oxide for the Chemo-Photothermal Therapy of Bacterial Infection in Bone Repair. *ACS Appl. Mater. Inter.* **14**, 21996–22005 (2022).
52. Shuai, C. et al. Silicon dioxide nanoparticles decorated on graphene oxide nanosheets and their application in poly (L-lactic acid) scaffold. *J. Adv. Res.* https://doi.org/10.1016/j.jare.2022.08.017 (2022).
53. Wei, C. et al. An overview of laser-based multiple metallic material additive manufacturing: from macro-to micro-scales. *Int. J. Extrem. Manuf.* **3**, 012003 (2020).
54. Feng, P. et al. Hydroxyapatite nanoparticles in situ grown on carbon nanotube as a reinforcement for poly (ε-caprolactone) bone scaffold. *Mater. Today Adv.* **15**, 100272 (2022).

55. Gao, C., Zeng, Z., Peng, S. & Shuai, C. Magnetostrictive bulk Fe-Ga alloys prepared by selective laser melting for biodegradable implant applications. *Mater. Des.* **220**, 110861 (2022).
56. Shuai, C. et al. Construction of Magnetic Nanochains to Achieve Magnetic Energy Coupling in Scaffold. (2022).
57. Beal, V. E., Erasenthiran, P., Hopkinson, N., Dickens, P. & Ahrens, C. H. The effect of scanning strategy on laser fusion of functionally graded H13/Cu materials. *Int. J. Adv. Manuf. Technol.* **30**, 844–852 (2006).
58. Jonkers, N., Van Dijk, W. J., Vonk, N. H., Van Dommelen, J. A. W. & Geers, M. G. D. Anisotropic mechanical properties of Selective Laser Sintered starch-based food. *J. Food Eng.* **318**, 110890 (2022).
59. Ochi, S., Kamishima, O., Mizusaki, J. & Kawamura, J. Investigation of proton diffusion in Nafion® 117 membrane by electrical conductivity and NMR. *Solid State Ion.* **180**, 580–584 (2009).
60. Huang, Z. et al. Biodegradability studies of poly (butylene succinate) composites filled with sugarcane rind fiber. *Polym. Test.* **66**, 319–326 (2018).
61. Tino, R. et al. Additive manufacturing in radiation oncology: a review of clinical practice, emerging trends and research opportunities. *Int. J. Extrem. Manuf.* **2**, 012003 (2020).
62. Shuai, C. et al. Water-responsive shape memory thermoplastic polyurethane scaffolds triggered at body temperature for bone defect repair. *Mater. Chem. Front.* **6**, 1456–1469 (2022).
63. Shuai, C. et al. Nitrogen-doped carbon-ZnO heterojunction derived from ZIF-8: a photocatalytic antibacterial strategy for scaffold. *Mater. Today. Nano* **18**, 100210 (2022).
64. Li, X. et al. 3D printing of hydroxyapatite/tricalcium phosphate scaffold with hierarchical porous structure for bone regeneration. *Bio-Des. Manuf.* **3**, 15–29 (2020).
65. Ock, J. & Li, W. A high-throughput three-dimensional cell culture platform for drug screening. *Bio-Des. Manuf.* **3**, 40–47 (2020).

ACKNOWLEDGEMENTS

This work was supported by the following funds: (1) The Natural Science Foundation of China (52275393, 51905553, 51935014, 82072084); (2) Hunan Provincial Natural Science Foundation of China (2021JJ20061, 2020JJ3047, 2019JJ50588); (3) The Project of State Key Laboratory of High Performance Complex Manufacturing; (4) Support by the Open Sharing Fund for the Large-scale Instruments and Equipments of Central South University; (5) The Wisdom Accumulation and Talent Cultivation Project of the Third xiangya hosipital of Central South University (YX202001); (6) The Fundamental Research Funds for the Central Universities of Central South University (CX20220298).

AUTHOR CONTRIBUTIONS

C.S. was responsible for conceptualization and supervision. Z.W. was responsible for methodology, formal analysis, data curation and writing—original draft. H.Z. was responsible for methodology. J.J. was responsible for software and validation; L.H. was responsible for resources. D.W. was responsible for investigation. S.C. was responsible for data curation. P.F. was responsible for conceptualization, project administration, funding acquisition and writing—review & editing.

COMPETING INTERESTS

The authors declare no competing interests.

ADDITIONAL INFORMATION

Correspondence and requests for materials should be addressed to Shijie Chen or Pei Feng.